

Gold Nanocages: A Novel Class of Multifunctional Nanomaterials for Theranostic Applications

By Jingyi Chen,* Miaoxin Yang, Qiang Zhang, Eun Chul Cho, Claire M. Coble, Chulhong Kim, Charles Glaus, Lihong V. Wang, Michael J. Welch, and Younan Xia*

Gold nanocages represent a novel class of nanostructures, well-suited for biomedical applications. They can be readily prepared via the galvanic replacement reaction between silver nanocubes and chloroauric acid. Their optical resonance peaks can be easily and precisely tuned to the near-infrared region from 650–900 nm, the transparent window for blood and soft tissue. Furthermore, their surface can be conveniently conjugated with various ligands for targeting cancer. In this feature article, we highlight recent advances in the large-scale synthesis of gold nanocages and their applications in cancer diagnosis and treatment. Specifically, we have scaled up the production of gold nanocages for *in vivo* studies and evaluated their tumor targeting capabilities. We have also demonstrated their use as contrast agents for photoacoustic tumor imaging and the mapping of sentinel lymph node, as photothermal transducers for cancer treatment, and as smart carriers for controlled release with a near-infrared laser.

1. Introduction

Gold (Au) nanostructures have attracted considerable attention in recent years for biomedical applications owing to their unique physical and chemical properties, as well as biocompatible properties.^[1] The medicinal use of Au can be traced back to the beginning of the 14th century, in products known as “potable gold” or “aurum potable” that could be internally consumed.^[2] Not until the 20th century was the medicinal efficacy of Au realized through controlled clinical trials for the treatment of rheumatoid arthritis.^[3] In 1950s, radioactive colloids made of ¹⁹⁸Au were introduced and explored by Hahn and co-workers to treat malignancies.^[4] In recent years, the rapid development in

nanoscience and nanotechnology brings the biomedical applications of Au colloids into a new era. New discoveries related to the preparation techniques and properties of Au nanostructures warrant further investigations into their use in biomedical research.

Gold particles with dimensions at the nanometer scale exhibit unique optical properties. When interacting with an electromagnetic field, the nanoparticle can strongly absorb and scatter light through the collective oscillation of conduction electrons confined within the nanoparticle, in a phenomenon widely known as localized surface plasmon resonance (LSPR). The resonant wavelength is highly dependent on the size, shape, structure (solid versus hollow), and surroundings of the Au nanoparticle.^[5] By tailoring these parameters,

one can readily manipulate the LSPR properties of Au nanoparticles for various applications, including biological sensing, optical imaging, photothermal treatment, as well as the controlled release of a drug.^[6] To maximize the penetration depth in soft tissues, the light source needs to be limited to the near-infrared (NIR) region from 650–900 nm, where the absorption by hemoglobin and water is negligible.^[7] A number of different Au nanostructures have been shown to exhibit LSPR peaks in the NIR region, with notable examples including core/shell, rod-shaped, or hollow nanostructures.^[8]

In this Feature Article, we focus our discussion on a novel class of Au nanostructures known as nanocages that are characterized by hollow interiors and ultrathin, porous walls. They can be easily prepared through the galvanic replacement reaction involving silver (Ag) nanostructures as sacrificial templates.^[9] In general, Au nanocages can be synthesized from four different types of Ag templates: single-crystal cubes with and without truncated corners, single-crystal octahedrons with truncated corners, and polycrystalline quasispheres (Figure 1). When Ag nanocubes with truncated corners are used as the templates, the resultant nanocages have pores preferentially located on {111} rather than {100} facets.^[10] By controlling the size and composition, the LSPR peak of Au nanocages can be precisely tuned throughout the visible and NIR regions to suit specific applications. Here we primarily highlight the photothermal properties

[*] Dr. J. Chen, M. Yang, Q. Zhang, Dr. E. C. Cho, C. M. Coble, Dr. C. Kim, Prof. L. V. Wang, Prof. Y. Xia
Department of Biomedical Engineering
Washington University in St. Louis
Saint Louis, MO 63130, USA
E-mail: chenj@seas.wustl.edu; xia@biomed.wustl.edu
Dr. C. Glaus, Prof. M. J. Welch
Department of Radiology
Washington University School of Medicine
Saint Louis, MO 63110, USA

DOI: 10.1002/adfm.201001329

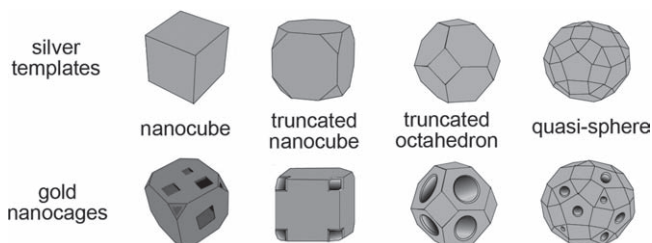
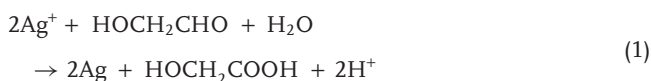


Figure 1. Schematic illustrations summarizing four major types of Au nanocages derived from different types of Ag templates: a single-crystal cube with sharp corners; a single-crystal cube with truncated corners; a single-crystal octahedron with truncated corners; and a polycrystalline, quasi-spherical particle.

(based on optical absorption) of Au nanocages for both cancer diagnosis and treatment. Our discussion includes the scale-up synthesis of Au nanocages, targeting of Au nanocages in vitro and in vivo, as well as their use as contrast agents for photoacoustic (PA) imaging, as photothermal transducers for cancer treatment, and as carriers for controlled release.

2. Synthesis of Gold Nanocages

There are two major technical requirements for Au nanocages: i) good uniformity in terms of both size and shape, as this will affect their optical properties and alter their biodistribution; ii) availability in large quantities as required for in vivo studies. As a result, one needs to produce Ag nanocubes with uniform, controllable sizes and quantities on the scale of grams per batch. A number of methods have been developed for the solution-phase synthesis of Ag nanocubes.^[11] Among these methods, the polyol reduction has proven to be a facile and robust route to high-quality Ag nanocubes in large quantities. In a typical polyol synthesis, ethylene glycol acts as both the solvent and source of reducing agent:^[12]



where the glycolaldehyde (HOCH_2CHO) is formed due to oxidation of ethylene glycol by the oxygen from air. The reduction typically generates seeds with different twin structures, including single-crystal, single-twinned, and multiple-twinned, which can further grow into cubes, right bipyramids, and pentagonal wires, respectively.^[13] To obtain Ag nanocubes in high yields, two approaches are generally used: i) removal of twinned seeds by oxidative etching; ii) fast reduction through the formation or addition of exotic seeds. In the first approach, oxidative etchants (e.g., Cl^- ions combined with O_2) are introduced to selectively eliminate the twinned seeds due to the high reactivity of defects on their surface.^[14] The remaining single-crystal seeds can lead to the growth of nanocubes with the assistance of poly(vinyl pyrrolidone) (PVP), which selectively binds to the $\{100\}$ facets. The oxidative etching is typically a slow process and the synthesis usually takes more than 10 h. The second approach is based on the formation of Ag_2S clusters as exotic seeds through the addition of NaHS or Na_2S to direct the nucleation of Ag atoms and catalyze the reduction of Ag^+ ions.^[15]



Jingyi Chen received a B.S. in Chemistry from Sun Yat-Sen University in China (1997), a M.A. in Chemistry from SUNY College at Buffalo (2002), and a Ph.D. in Analytical Chemistry with Professor Younan Xia from the University of Washington (2006). She then worked as a postdoctoral fellow at Brookhaven National

Laboratory. She worked as a Research Assistant Professor of Biomedical Engineering at Washington University in St. Louis from May 2008 to July 2010. She is currently an Assistant Professor of Chemistry and Biochemistry at the University of Arkansas, Fayetteville. Her research interests include the synthesis and characterization of nanostructured materials for clean energy and biomedical applications.



Younan Xia was born in Jiangsu, China, in 1965. He received a B.S. in Chemical Physics from the University of Science and Technology of China (USTC) in 1987 and worked as a graduate student for four years at the Fujian Institute of Research on the Structure of Matter, Chinese Academy of Sciences. In 1993, he received a M.S. in

Inorganic Chemistry from the University of Pennsylvania (with the late Professor Alan G. MacDiarmid), and in 1996 a Ph.D. in Physical Chemistry from Harvard University (with Professor George M. Whitesides). After a short stint as a postdoctoral fellow with Professors George M. Whitesides and Mara Prentiss, he started as an Assistant Professor of Chemistry at the University of Washington in Seattle. He was promoted to Associated Professor and Professor in 2002 and 2004, respectively. He moved to Washington University in

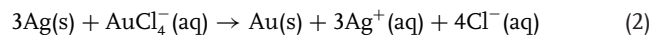
St. Louis in 2007 and is the James M. McKelvey Professor for Advanced Materials in the School of Engineering. His research interests include nanostructured materials, nanomedicine, biomaterials, tissue engineering, self-assembly, photonic crystals, colloidal science, surface modification, and electrospinning.

The rapid reduction effectively limits the formation of twinned seeds, thus facilitating the formation of thermodynamically favored, single-crystal, cubo-octahedral seeds and the subsequent growth of nanocubes.

The traditional polyol method uses AgNO_3 as a precursor to elemental Ag; the yield of Ag nanocubes is highly sensitive to

many reaction conditions, including impurities and the amount of oxygen. The nitrate group is also an oxidizer that may cause etching of the single-crystal seeds and thus lead to poor reproducibility of the synthesis. Most recently, we found that the polyol synthesis of Ag nanocubes could become highly robust and reproducible by switching the precursor from AgNO₃ to CF₃COOAg.^[16] Similar to our previous findings, the presence of trace amounts of NaHS and HCl also allows the rapid nucleation of single-crystal seeds and elimination of the twinned seeds in this new protocol. Meanwhile, the CF₃COO⁻ group has no etching power for the single-crystal Ag seeds and thus no effect on the crystal growth. **Figure 2A** shows a photograph of the experimental set up. Upon preheating ethylene glycol to 150 °C and addition of the reactants, the reaction was allowed to proceed at 150 °C for about 1 h. The relative mild reduction rate allowed us to record the spectra of aliquots sampled from the reaction solution to obtain the desired size of nanocubes in the range of 30 to 70 nm, as the position of the LSPR peak is largely determined by the size of the nanocubes. Using this method, we can routinely prepare high-quality Ag nanocubes (**Figure 2B**) in relatively large quantities (e.g., 2 × 10¹² nanocubes or 3 × 10⁻¹¹ mol or 30 pmol of 40-nm Ag cubes) within approximately one hour.

Gold nanocages are prepared via the galvanic replacement reaction between Ag templates and HAuCl₄, which is driven by the difference in electrochemical potential between Ag/Ag⁺ (0.80 V) and Au/AuCl₄⁻ (1.00 V).^[17]



The reaction can, in principle, be scaled up to any volume. In practice, the entire batch of Ag nanocubes (30 pmol of

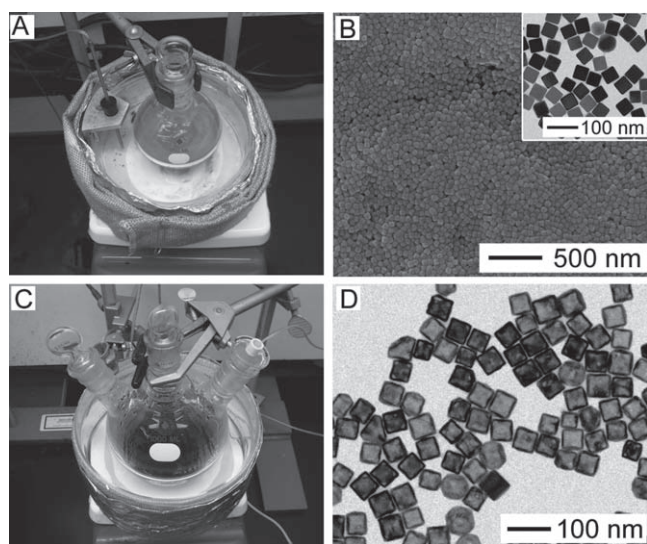


Figure 2. A) Schematic image illustrating the setup used for synthesizing Ag nanocubes on a scale of 0.1 g per batch. B) SEM image of the as-synthesized Ag nanocubes, which were 45 nm in edge length. The inset shows a transmission electron microscopy (TEM) image of the same sample. C) Schematic illustrating the setup used for synthesizing Au nanocages on a scale of 0.1 g Ag nanocubes. D) TEM image of a typical sample of Au nanocages, which were 55 nm in edge length.

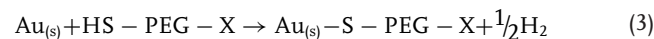
40-nm Ag cubes) were transformed into Au nanocages in a single reaction by adding 0.75 mM HAuCl₄ solution at a rate of 45 mL h⁻¹. **Figure 2C** shows the experimental setup of a scale-up production in a 500 mL round-bottom flask. The reaction process was monitored by visualization of the color changes from brown-yellow (≈400 nm) to deep blue (800 nm) and taking UV-vis spectra from aliquots sampled from the reaction solution at different time points. **Figure 2D** shows a representative TEM image of 50-nm Au nanocages with an LSPR peak at 800 nm that matches the wavelength of the diode laser used to evaluate their photothermal effect. To maintain epitaxial growth for the Au atoms on the Ag nanocubes, the reaction temperature was maintained at 100 °C to avoid any precipitation of AgCl (the solubility product at 100 °C was $K_{sp} = 1 \times 10^{-6}$) during galvanic replacement. Once cooled down to room temperature, the AgCl solid could be dissolved by adding a saturated NaCl solution through the formation of soluble coordination complex with chloride and subsequently be removed with the supernatant after centrifugation.^[18]

3. Targeted Delivery of Au Nanocages

For both diagnostic and therapeutic applications, it is critical to deliver Au nanocages exclusively to the malignant site. In this regard, it is necessary to engineer the size, shape, and surface properties of Au nanocages to optimize their targeting efficacy and uptake by the desired biological system.

3.1. Surface Modification of Au Nanocages

Two strategies are generally used for chemical functionalization of nanoparticles: formation of the nanoparticles in the presence of thiols and post-synthesis ligand exchange.^[19] The latter has been used for the surface modification of Au nanocages. After galvanic replacement, the surface of Au nanocages should be covered with PVP, which is a biocompatible polymer. The pyridone units can bridge adjacent metal atoms on the nanoparticle surface through the formation of coordination bonds via amine-*N* and carbonyl-*O* donors.^[20] For targeting purposes, PVP can be displaced by a thiol-terminated polyethylene glycol (HS-PEG-X, where X is a functional group that is readily coupled with targeting moiety) through chemisorptions:



Similarly, disulfides can also substitute PVP through the S-S bond dissociation, adsorbing on the surface as two separate thiolate species. The strength of the Au-S bond is estimated to be roughly 40 kcal mol⁻¹ or 167 kJ mol⁻¹, which is approximately a factor of 2 less than that of C-C bond.^[19,21] The Au-S bond is rather stable under physiological conditions. Targeting molecules, such as antibodies, peptides, aptamers, and small molecules (e.g., vitamins or inhibitors), can be conjugated to Au nanocages through the distal group of the immobilized PEG chain. The most common method is to react the primary amine with carboxylic acid via a coupling agent such as 1-ethyl-3-(3-dimethylaminopropyl) carbodiimide hydrochloride (EDC) or *N*-hydroxysulfosuccinimide (sulfo-NHS) in a buffered solution.

3.2. Cellular Uptake of Au Nanocages

Understanding the interactions between nanoparticles and cells is key to rationally designing nanoparticles for medical applications. To examine the effects of size and surface chemistry of Au nanocages on their cellular uptake, we have studied Au nanocages of two different sizes, 33 and 55 nm.^[22] These nanocages were functionalized with PEG, antibody (anti-HER2), and poly(allyaminehydrochloride) (PAA), respectively (Figure 3A). The uptake of these nanocages was investigated using the SK-BR-3 breast cancer cell line which is known to overexpress epidermal growth factor receptor 2 (EGFR2 or HER2) (Figure 3B). In general, the 33-nm nanocages had a higher uptake than the 55-nm nanocages. For the dependence on surface chemistry, the uptake of Au nanocages decreased in the order of PAA >> anti-HER2 > PEG. The much higher uptake of the PAA-coated nanocages can be explained by two reasons: the high affinity of PAA coating to the cell membrane due to the electrostatic attraction,^[23] and disruption of the cell membrane through an ATP-independent process.^[24] The anti-HER2 coated nanocages had a higher affinity than the PEGylated nanocages due to the interaction between anti-HER2 and its receptor.

To differentiate the surface-bounded nanocages from the internalized ones, the cells were etched with I₂/KI to selectively remove surface-bound nanocages.^[25] The fraction of Au nanocages on the cell surface increased in the order of PAA > anti-HER2 ≥ PEG. The uptake of nanoparticles generally

involves two steps: i) adhesion to the cell surface, followed by ii) internalization. The adhesion usually is the rate-limiting step. The anti-fouling nature of PEG makes it hardly adsorb onto the cell membrane, and thus their adhesion rate appeared to be the lowest among these three samples with different surface groups. As soon as they adsorbed, the PEGylated nanocages were internalized by the cells. On the other hand, 70–80% of the anti-HER2-coated nanocages were internalized, whereas a considerable amount of PAA-coated nanocages remained on the cell surface. These experimental results may give some guidance for the cellular targeting of nanoparticles once they are accumulated at the tumor site.

3.3. In Vivo Targeting of Gold Nanocages

Passive and active targeting are the two general methods for delivering nanoparticles to the target area of the body.^[26] Passive targeting relies on the accumulation of nanoparticles in a tumor or inflamed tissue by the enhanced permeability and retention (EPR) effect associated with the leaky vasculature and the dysfunctional lymphatic system of a tumor. On the other hand, active targeting takes advantage of the highly selective interaction between the ligand immobilized on the nanoparticles and the specific receptor overexpressed on the surface of tumor cells to deliver the nanoparticles to the targeted cells after extravasation.

We recently evaluated the passive targeting capabilities of PEGylated Au nanocages in a subcutaneous tumor mouse model. The Au nanocages with an edge length of 48 nm and an LSPR peak at around 800 nm were functionalized with a monolayer of PEG of 5000 in molecular weight at a coverage of 20 000 PEG per nanocage. The mice were divided into three groups ($n = 4$ per group) and administered intravenously with 100 μL of 9.2 mg mL⁻¹ (14 nm or 8.4×10^{12} particles mL⁻¹) PEGylated Au nanocages. Figure 4A plots the distributions of the PEGylated Au nanocages in various organs at three different times after intravenous injection. The particle concentration in the blood decreased from $40.8 \pm 14.0\%$ ID g⁻¹ at 1 h post injection to $34.5 \pm 3.0\%$ ID g⁻¹ at 5 h post injection and could still maintain a level of $10.8 \pm 3.1\%$ ID g⁻¹ at 24 h post injection. As the nanocages were cleared from the blood, the Au content in the normal tissues also decreased, from $1.38 \pm 0.26\%$ ID g⁻¹ at 1 h post injection to $0.95 \pm 0.24\%$ ID g⁻¹ at 24 h post injection and $2.16 \pm 0.76\%$ ID g⁻¹ at 1 h post injection to $0.98 \pm 0.45\%$ ID g⁻¹ at 24 h post injection, for muscle and fat, respectively. The uptake of the PEGylated Au nanocages by the liver only slightly increased from $6.8 \pm 1.9\%$ ID g⁻¹ at 1 h post injection to $12.1 \pm 4.9\%$ ID g⁻¹ at 24 h post injection, while the uptake by the spleen dramatically increased from $5.1 \pm 2.4\%$ ID g⁻¹ at 1 h to $43 \pm 7.9\%$ ID g⁻¹ at 24 h. The results were in agreement with previous studies with polymeric or solid Au nanoparticles: that is, the uptake by the spleen is often more significant than that by liver once the nanoparticles had been functionalized with PEG.^[27] This result implies that the PEGylated nanocages were filtered by the venous sinusoidal system of the spleen.^[28] Since the PEGylated Au nanocages had a prolonged circulation time in the blood, they could accumulate at the tumor site as a result of the EPR effect associated with the leaky vasculature of a tumor.

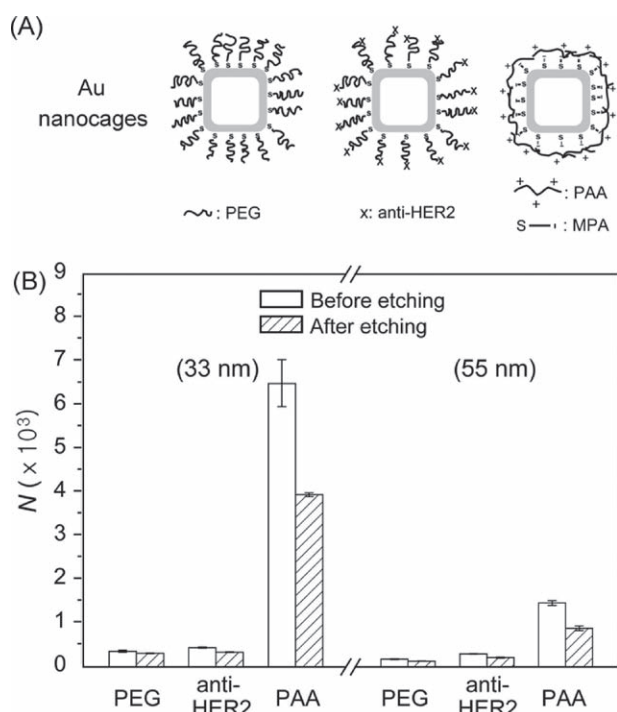


Figure 3. A) Schematic illustrating Au nanocages whose surface had been modified with various functional groups. B) Uptake of surface-modified Au nanocages by SK-BR-3 cells after incubation at 37 °C for 24 h, followed by etching with 0.34 mM I₂ for 5 min. N represents the number of Au nanocages taken up per cell. The number of samples tested for each data point was six. Reproduced with permission.^[22]

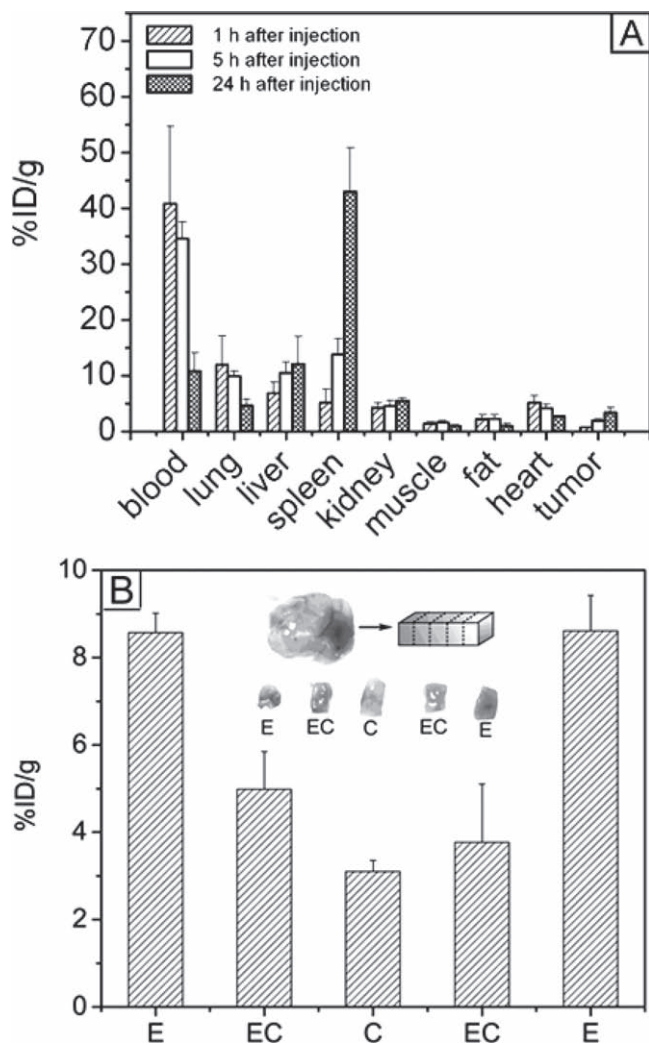


Figure 4. A) Biodistribution of PEGylated Au nanocages in tumor-bearing mice intravenously administrated with 100 μL of the nanocages (8.4×10^{12} particles mL^{-1}). The amount of Au in the tissue samples were analyzed by ICP-MS at three different time points. Each data point represents the mean value for $n = 4$ and the bar is standard deviation for the mean. B) Distribution of the PEGylated Au nanocages in the tumor. Note that E, C and EC represent edge, center, and the region between edge and center, respectively. Each data point represents the mean value for $n = 3$ and the bar is the standard deviation for the mean. Reproduced with permission.^[41]

In this study, we found that the amount of the PEGylated Au nanocages in the tumor increased from $0.8 \pm 0.1\%$ ID g^{-1} at 1 h, to $1.9 \pm 0.3\%$ ID g^{-1} at 5 h and $3.4 \pm 0.9\%$ ID g^{-1} at 24 h. To examine the spatial distribution of the nanocages in a tumor, a rectangular core through each tumor was sectioned into five pieces. The edges were found to contain more nanocages than the center portion of the tumor (Figure 4B). During the course of four days, the PEGylated Au nanocages gradually penetrated through the leaky blood vessels of the tumor and diffused into the interstitium region of the tumor.^[29]

To demonstrate active targeting, we recently functionalized Au nanocages with a melanoma specific peptide, [Nle⁴, D-Phe⁷]- α -melanocyte stimulating hormone ([Nle⁴, D-Phe⁷]- α -MSH),

through a PEG spacer to form [Nle⁴, D-Phe⁷]- α -MSH-AuNCs and compared their accumulation in tumor relative to the PEGylated Au nanocages (PEG-AuNCs) using the non-invasive PA imaging technique.^[30] Figure 5A plots the PA signal enhancement in the melanomas as a function of post-injection time. At $t = 6$ h post injection, the targeting efficiency of [Nle⁴, D-Phe⁷]- α -MSH-AuNCs was about three times higher than that of PEG-AuNCs. The results agreed with the ICP-MS analyses of the Au content present in the tumors (Figure 5B). From this data, we can conclude that Au nanocages can be actively delivered to a tumor target by modifying their surface with a ligand

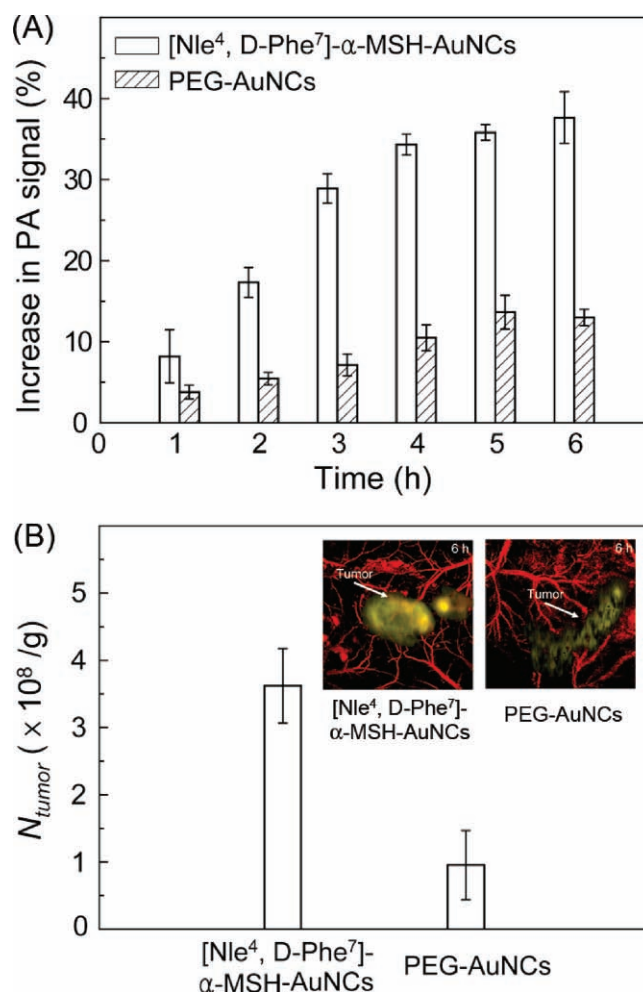


Figure 5. A) Time-course changes (%) in PA amplitude after intravenous injection of [Nle⁴,D-Phe⁷]- α -MSH- and PEG-AuNCs ($n = 4$ mice for each group). The PA signals increased up to $38 \pm 6\%$ for [Nle⁴,D-Phe⁷]- α -MSH-AuNCs while the maximum signal increase only reached $13 \pm 2\%$ for PEG-AuNCs at a post-injection time of 6 h ($p < 0.0001$). B) The average number of AuNCs accumulated in the melanomas dissected at 6 h post-injection for the two types of AuNCs as measured by ICP-MS. Here N_{tumor} denotes the number of AuNCs per unit tumor mass (g). The average number of [Nle⁴,D-Phe⁷]- α -MSH-AuNCs per tumor mass ($3.6 \pm 1.0 \times 10^8$ AuNCs g^{-1}) was 3.6 times ($p = 0.02$) that of PEG-AuNCs ($1.0 \pm 0.1 \times 10^8$ AuNCs g^{-1}). The inset shows the PA images of the melanoma at 6 h post-injection of [Nle⁴,D-Phe⁷]- α -MSH- and PEG-AuNCs, respectively. Reproduced with permission.^[30] Copyright 2010, American Chemical Society.

that specifically binds to a biomarker overexpressed on the surface of the tumor.

4. Gold Nanocages for Photoacoustic Imaging

Photoacoustic imaging represents an emerging hybrid modality involving both optical and ultrasonic techniques that can provide high sensitivity, high resolution, and deep penetration.^[31] In PA imaging, a short-pulsed laser beam is used to irradiate the tissue and ultrasound signals are collected to generate a three-dimensional image of the anatomical structures. The amplitude of the PA signal is proportional to optical absorption. Nanoparticles with strong optical absorption have been explored as contrast agents, and they can be classified into two categories based on the physical mechanism of light absorption: plasmonic nanoparticles (e.g., Au nanocages) and dye-containing nanoparticles.^[32] Owing to their strong, tunable absorption in the NIR region, high stability, and compact sizes, Au nanocages are ideal contrast agents for PA imaging.

4.1. Measuring the Absorption Cross Sections of Gold Nanocages

The LSPR of plasmonic nanoparticles consists of two components: absorption and scattering. The magnitude of absorption plays a central role in PA imaging and photothermal conversion, while the scattering power is essential for other imaging modalities such as optical coherence tomography (OCT) and dark-field optical microscopy.^[33] Although theoretical calculations can give the absorption and scattering cross sections, experimental measurements of these values have been difficult. We recently developed a method based on PA imaging for directly measuring the absorption cross section, where the absorption coefficients of Au nanostructures are derived from the PA signal amplitudes using a calibration method.^[34] In a typical experiment, the absorption coefficient of a sample of Au nanostructures was obtained from the PA signal by benchmarking against a linear calibration curve (PA signal versus absorption coefficient) derived from a set of aqueous solutions of methylene blue (an organic dye with a known absorption cross section) with varying concentrations.

Figure 6A shows a setup of the PA imaging system used for the optical measurements. Three Tygon tubes were embedded in an optically scattering medium and filled with aqueous suspensions of Au nanostructures or aqueous solutions of methylene blue. When the suspensions were illuminated with light scattered from the laser, PA signals were generated through thermo-elastic expansion due to absorption of light. A single-element 5-MHz ultrasound transducer was used to detect the PA signals, with spatial resolutions of 138 μm in the axial direction and 490 μm in the transverse direction. The suspension was removed from the tube after each measurement, and fresh suspensions were added into the same tube for additional measurements. For each sample, the PA signals were averaged over 20 different positions along the Y direction. Figure 6B shows typical depth-resolved, two-dimensional PA images (B-scan) of Au nanocages with an edge length of 45 nm and at

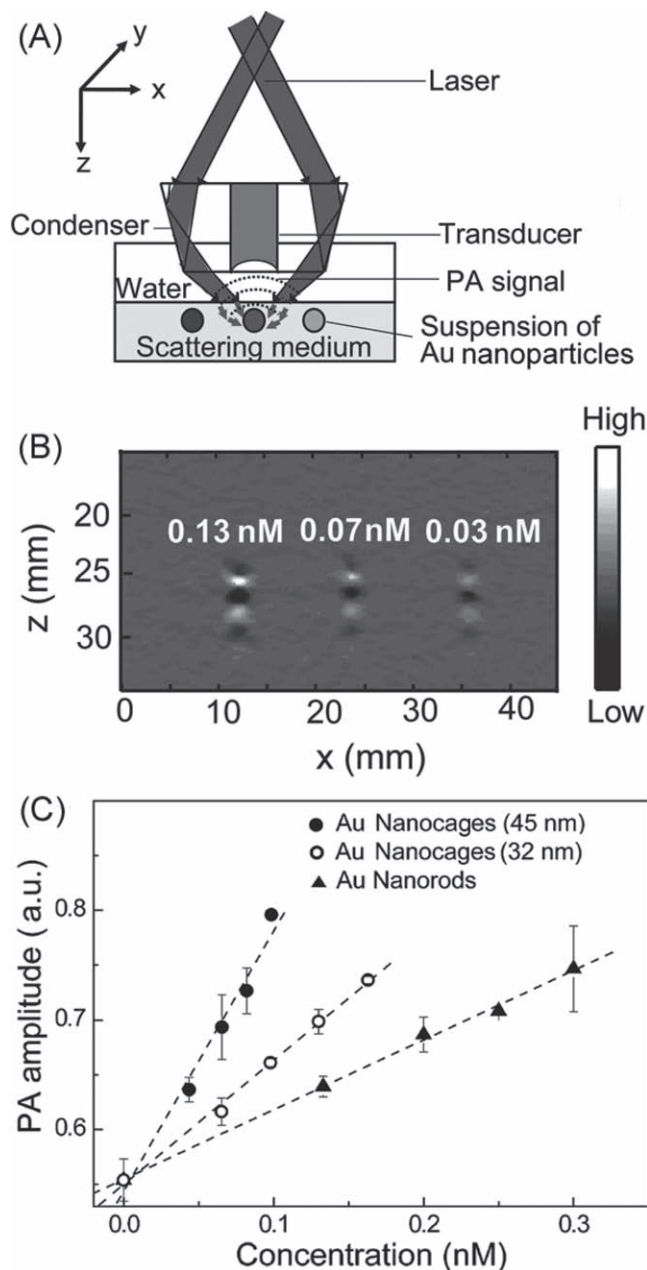


Figure 6. A) Schematic illustrating the experimental setup of the PA imaging system. B) A typical depth-resolved B-scan PA image (x - z scan) of the suspensions of Au nanocages. C) Plots showing PA signal amplitude as a function of concentration for three types of nanostructures. Reproduced with permission.^[34] Copyright 2009, American Chemical Society.

concentrations of 0.13, 0.07, and 0.03 nM. The PA signals decreased as the concentration was reduced (Figure 6C). Using a calibration curve derived from methylene blue, the PA signal amplitudes could be converted into the absorption coefficients and further to the absorption cross section by dividing it with the concentration of the Au nanocages. The measured absorption cross sections of the Au nanocages (with LSPR peak at ≈ 650 nm) were: $3.0 \times 10^{-15} \text{ m}^2$ and $6.0 \times 10^{-15} \text{ m}^2$ for 30-nm

and 45-nm nanocages, respectively. Both values were larger than that ($1.9 \times 10^{-15} \text{ m}^2$) of Au nanorods with LSPR at $\approx 650 \text{ nm}$. Using this method, we can directly compare the absorption cross sections of different types of nanostructures and rationally design plasmonic nanostructures to maximize the photothermal effect.

4.2. Gold Nanocages for Photoacoustic Mapping of Sentinel Lymph Node

The large absorption cross sections of Au nanocages in the NIR region make them ideal imaging contrast agents for cancer diagnosis by, for example, PA mapping of sentinel lymph nodes (SLN).^[35] SLN mapping is required prior to SLN biopsy for the physician to identify the target. Such a procedure is widely used to determine whether cancer has spread from the primary tumor in a breast cancer patient. As compared to standard techniques using radioactive colloids and other imaging modalities (e.g., MRI and optical imaging) being developed,^[36] PA imaging can provide both high sensitivity, high resolution, and deep imaging depth for SLN mapping. Methylene blue dye is commonly used as a contrast agent for SLN mapping to assist needle biopsy. However, due to the very small hydrodynamic diameter of dye molecule ($<2 \text{ nm}$),^[37] it may quickly stain the distal or second tier lymph nodes, resulting in removal of more lymph nodes as opposed to the true SLN. To solve this problem, Au nanocages with tunable LSPR peaks in 650–900 nm and sizes ($>10 \text{ nm}$) can serve as contrast agents for SLN mapping. Additionally, the absorption cross section of the Au nanocage is five order of magnitude higher than that of the absorbing dye molecule, making the Au nanocages ideal as contrast agent for PA imaging.^[34]

Figure 7A–D, shows the PA images of SLN before and after injection of 0.2 pmol of Au nanocages (2 nM, 100 μL) into the forepaw pad of a rat at different time points. The PA signal from the SLN started to be detected at 5 min post injection. The contrast of the SLN gradually increased and reached a plateau at $\approx 2 \text{ h}$. After imaging, we dissected the SLN and quantified the number of nanocages ex vivo. Most nanocages appeared to accumulate in the subcapsular sinus of the node ($6.9 \pm 0.29 \text{ nM}$) and few drained to the trabecular sinus ($0.15 \pm 0.016 \text{ nM}$). This may be caused by the function of the lymph node as a filter. In humans, the top surface of SLN is located on average $12 \pm 5 \text{ mm}$ underneath the skin.^[35] To meet the clinical depth, we demonstrated the depth capability of this imaging technique by placing chicken breast tissue on top of the rat skin. We were able to detect the SLN 33 mm below the tissue surface (Figure 7E). The PA signals were found to exponentially decay with depth (Figure 7F). The Au nanocage-enabled PA imaging offers a noninvasive and nonionizing technique to map SLNs with high spatial resolution at low cost. With the aid of targeting molecules conjugated to the surface of the nanocages, this method can potentially provide a new tool for noninvasive SLN identification of metastases.

5. Gold Nanocages for Photothermal Treatment and Drug Release

In addition to cancer diagnosis, the photothermal capabilities of Au nanocages make them attractive for cancer treatment. Based

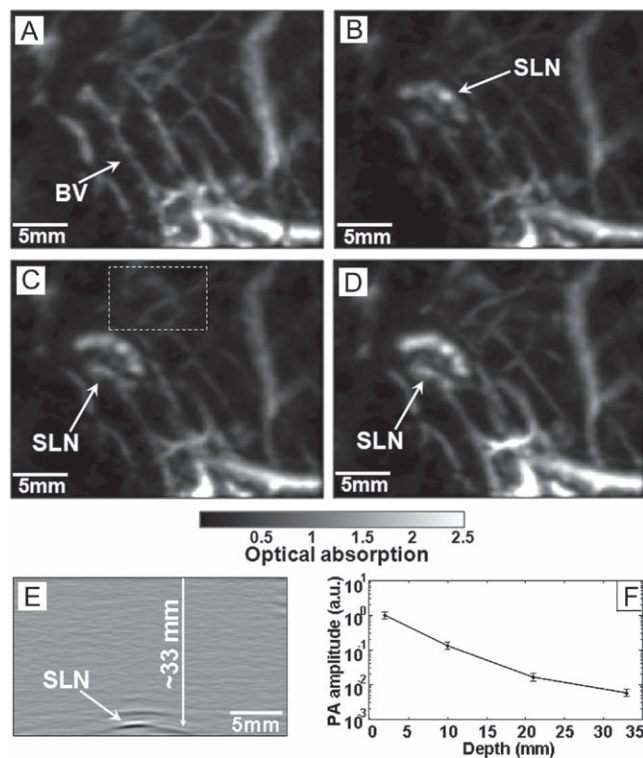


Figure 7. PA images acquired before (A) and after (B–D) the injection of Au nanocages: B) 5 min (SLN started to appear); C) 59 min; and D) 194 min. All images were acquired without signal averaging. PA signals from the SLN were normalized by those from adjacent blood vessels (the dotted box in Figure 7C) to minimize the ultrasonic focal effect. E) PA image (B-scan) of the SLN located 33 mm underneath the skin. F) The amplitude of PA signal as a function of imaging depth. The error bar represents standard deviation. BV, blood vessels; SLN, sentinel lymph node. Reproduced with permission.^[35] Copyright 2009 American Chemical Society.

on ultrafast laser spectroscopy studies, the electrons of Au nanocages can be excited by a pulsed laser to become extremely hot electrons on a picosecond timescale. The hot electrons subsequently equilibrate with the lattice through an electron-phonon coupling process and then transfer the energy to the surroundings (i.e., the suspension medium) on a timescale of 10–100 ps.^[38] When the Au nanocages are specifically attached to cancer cells through tumor targeting moieties, the neoplastic cells can be effectively killed upon irradiation with a NIR laser. The photothermal effect of Au nanocages can also be used to trigger the conformation of heat-sensitive polymer chains tethered to the surface and thus control the release of encapsulated drug molecules for chemotherapy.

5.1. Measurement of Photothermal Conversion

For a given photothermal material, it is important to evaluate a number of factors, such as the concentration of material, power density of the laser, and irradiation time, to better guide both in vitro and in vivo studies. We recently examined the increase in temperature as a function of Au nanocage concentration upon

irradiation by a diode laser at 0.5 W cm^{-2} up to 10 min (Figure 8A). Without nanocages, the temperature of the aqueous suspension only increased by $2.3 \text{ }^\circ\text{C}$ after exposure to a total light dose of 300 J cm^{-2} . Such a temperature increase should not cause any adverse effects to the cells or tissue because the suspension temperature is still below $42 \text{ }^\circ\text{C}$, a threshold temperature that will cause biomacromolecules (e.g., proteins) to denature.^[39] After 10 min exposure to a laser beam at 0.5 W cm^{-2} , the temperature increases were 6.1 and $23.8 \text{ }^\circ\text{C}$ for 1 and $10 \text{ } \mu\text{M}$ nanocages, respectively. Considering the body temperature as $37 \text{ }^\circ\text{C}$, the final temperatures were 43.1 and $60.8 \text{ }^\circ\text{C}$ for 1 and $10 \text{ } \mu\text{M}$ samples (in terms of particles), respectively. It is clear that a concentration of nanocages on the μM level is sufficient to have therapeutic effect on cancer cells through the photothermal treatment. Note that the Au nanocages could sustain their structures and optical properties for prolonged irradiation by a diode laser in an aqueous medium due to the rapid heat dissipation. No change was observed in the optical spectrum after exposure to the diode laser to a total light dose of 600 J cm^{-2} (Figure 8B). This observation indicates that the irradiation had essentially

no impact on the structure of the nanocages. Although the heat dissipation in solution is different from that in a soft tissue containing 70% water content,^[40] the results could provide us valuable information to determine the dose of nanocages and irradiation parameters for in vivo study.

5.2. Photothermal Cancer Treatment

We recently investigated the use of Au nanocages as a class of photothermal transducers to treat tumor-bearing mice.^[41] The mice with a tumor size of $\approx 10 \times 10 \text{ mm}^2$ on both flanks were divided into two groups ($n = 4$ per group) with Group 1 being administrated intravenously with $100 \text{ } \mu\text{L}$ of 10 mg mL^{-1} (15 nm or 9×10^{12} particles per mL) PEGylated Au nanocages and Group 2 being administrated with $100 \text{ } \mu\text{L}$ saline. At 72 h post injection, the tumor on the right flank of each mouse was irradiated with a 808-nm diode laser at a power density of 0.7 W cm^{-2} for 10 min (Figure 9A). During the treatment, the tumors of mice injected with PEGylated Au nanocages were rapidly heated to temperatures over $55 \text{ }^\circ\text{C}$ (Figure 9B–E). In contrast, the saline-injected mice showed much less local temperature increases with maximum surface temperature $<40 \text{ }^\circ\text{C}$ during the laser irradiation (Figure 9F–I).

To evaluate the treatment response, we used the [^{18}F] fluorodeoxyglucose (^{18}F -FDG) positron emission tomography (PET) to monitor the changes in metabolic activity before and after photothermal ablation (Figure 10). The FDG serves as a surrogate marker for tumor metabolism and provides better evaluation than the Responsive Evaluation Criteria in Solid Tumors (RECIST).^[41] For mice injected with PEGylated Au nanocages, the ^{18}F -FDG PET study showed remarkable reduction in FDG uptake for the tumor on the right flank at 24 h post treatment as compared to no treatment. In contrast, the tumor on the left flank without laser treatment showed no significant difference for the FDG uptake at 0 h and 24 h. Similar results with little difference in FDG uptake at 0 h and 24 h were also found in the control mice injected with saline for the tumor (right) with laser treatment and the tumor (left) with no laser treatment. We then normalized the signal of the right tumor to that of the left tumor to minimize the variation of FDG uptake at different time points. The normalized value was 0.3 after irradiation for the mice injected with Au nanocages as opposed to 1 before irradiation, indicating a decrease in metabolic activity by 70% (Figure 10E). For the saline-injected mice, the normalized value of FDG uptake was close to 1 before and after laser treatment. The ^{18}F -FDG PET study clearly indicated high efficacy of photothermal treatment based on the Au nanocages. Both the dose of nanocages and the light can be optimized to completely eradicate the tumor in future studies.

5.3. Controlled Release of Drug

Drug molecules can also be caged in the interiors of the Au nanocages and released as controlled by NIR light through the photothermal effect.^[43] Figure 11A shows the cartoon of such a drug delivery system based on smart polymer covered Au nanocages. The smart polymer, poly(N-isopropylacrylamide)

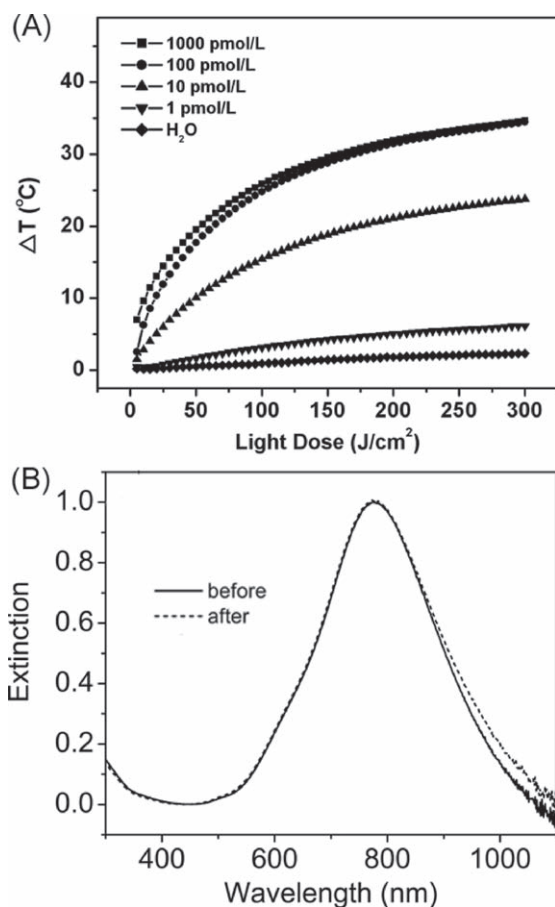


Figure 8. A) Plots of temperature increase for suspensions of Au nanocages with different concentrations as a function of light dose for a diode laser with a center wavelength at 808 nm. B) UV-vis-NIR spectra of the suspensions of Au nanocages before (solid line) and after (dashed line) irradiation with the diode laser at a power density of 1 W cm^{-2} for 10 min. Reproduced with permission.^[41]

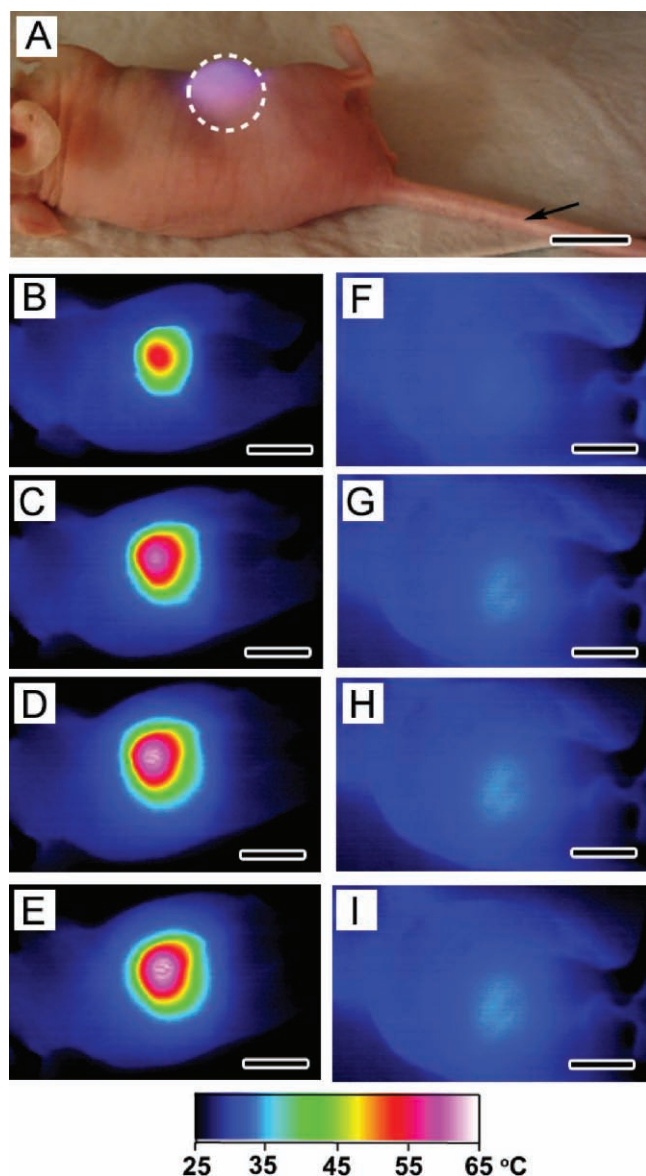


Figure 9. A) Photograph of a tumor-bearing mouse undergoing photothermal treatment. 100 μL of PEGylated nanocages at a concentration of 9×10^{12} particles per mL or saline was administered intravenously through the tail vein as indicated by an arrow. After the nanocages had been cleared from the circulation (72 h after injection), the tumor on the right flank was irradiated by the diode laser at 0.7 W cm^{-2} with a beam size indicated by the dashed circle. B–G) Thermographic images of (B–E) nanocage-injected and (F–I) saline-injected tumor-bearing mice at different time points: B,E) 1 min; C,F) 3 mi; D,G) 5 min; and E, I) 10 min. The scale bar is 5 mm. Reproduced with permission.^[41]

(pNIPAAm), or its derivatives, were grafted to the surface of the Au nanocages through thiolate linkages. These polymers can change conformation in response to small variations in temperature at a threshold known as the low critical solution temperature (LCST).^[44] Upon exposure to a laser beam whose wavelength matches the LSPR peak of the Au nanocages, the light will be absorbed and converted into heat. Through heat dissipation, the temperature rise will cause the polymer chains

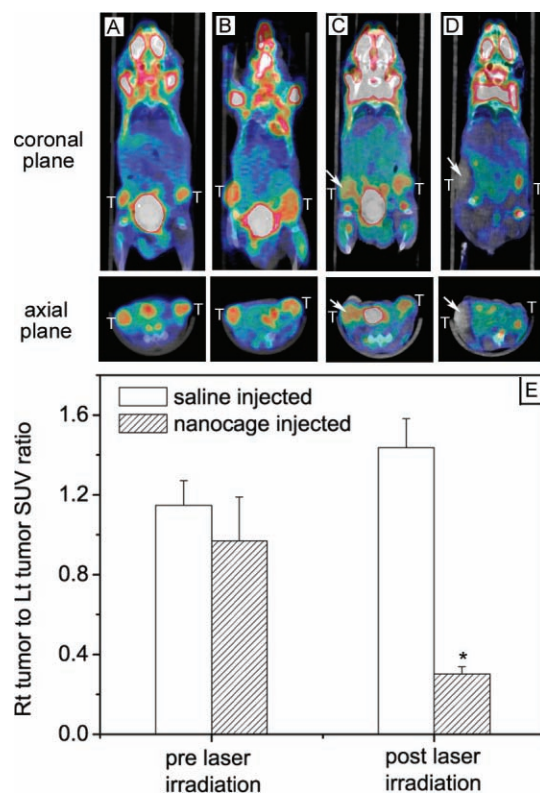


Figure 10. ^{18}F -FDG PET/CT co-registered images of mice intravenously administered with either saline or Au nanocages, followed by laser treatment: A) a saline-injected mouse prior to laser irradiation; B) a nanocage-injected mouse prior to laser irradiation; C) a saline-injected mouse after laser irradiation; and D) a nanocage-injected mouse after laser irradiation. The white arrows indicated the tumors that were exposed to the diode laser at a power density of 0.7 W cm^{-2} for 10 min. E) A plot showing the ratios of laser-treated tumor (Rt tumor) to non-treated tumor (Lt tumor) ^{18}F -FDG standardized uptake values (SUV, $P < 0.001$). Reproduced with permission.^[41]

to collapse and expose the pores on the nanocages, resulting in the release of the drugs. Once the laser is turned off, the heating will cease. The temperature drop will bring polymer conformation to its original, extended conformation. By turning the light on and off, we can remotely control the release of drug molecules through the Au nanocage-based photothermal effect.

To demonstrate this concept, we trapped an anticancer drug molecule, doxorubicin (Dox), in the polymer-coated nanocages and monitored its release in vitro. By incorporating acrylamide to the polymer chain, the LCST of the copolymer was adjusted to $39 \text{ }^\circ\text{C}$, which is above the body temperature, but below the hyperthermia temperature. Figure 11B shows a release profile of Dox from the Au nanocages by heating at $45 \text{ }^\circ\text{C}$. A fast release of Dox was observed when the sample was heated. We then tested the controlled release of Dox in an in vitro study by incubating the Dox-loaded nanocages with breast cancer cells. The wells containing the cancer cells and Dox-loaded nanocages were subject to pulsed laser irradiation at a power density of 20 mW cm^{-2} for 2 and 5 min, respectively (Figure 11B). The percentage of the live cancer cells decreased with increased laser exposure time. In contrast, little change was observed

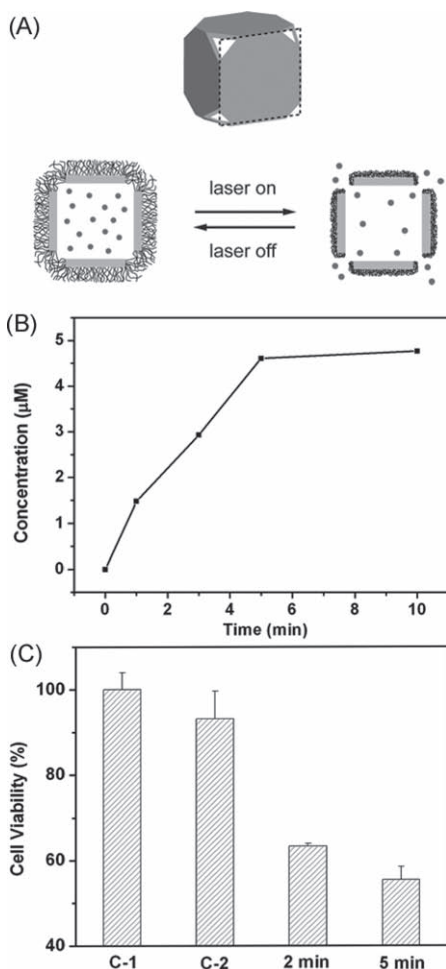


Figure 11. A) Schematic illustrating how the new release system works. Upon exposure to a NIR laser, the light is absorbed by the nanocage and converted into heat, triggering the smart polymer to collapse and thus release the pre-loaded drug. When the laser is turned off, the polymer chains will relax back to the extended conformation and terminate the release. B) A plot of the concentrations of Dox released from the Au nanocages upon heating at 45 °C for different periods of time. C) Cell viability for samples after going through different treatments: C-1) cells irradiated with a pulsed NIR laser for 2 min in the absence of Au nanocages; C-2) cells irradiated with the laser for 2 min in the presence of empty Au nanocages; and (2/5 min) cells irradiated with the laser for 2 and 5 min in the presence of Dox-loaded Au nanocages. A power density of 20 mW cm⁻² was employed for all these studies. Reproduced with permission.^[43] Copyright 2009, Nature Publishing Group.

for the cell viability in the absence of Au nanocages when the cells were exposed to laser for 2 min. Under the same irradiation condition, the cells with Au nanocages alone showed slight reduction in cell viability possibly due to the photothermal effect. The smart polymer-coated Au nanocages can thus potentially allow us to release drug molecules with high temporal/spatial resolutions in a controlled manner.

6. Conclusion and Perspective

Nanotechnology may provide a better way to fight cancer which accounts for the second cause of deaths in the United State.^[45] We

have developed a new platform based on Au nanocages for cancer diagnosis and treatment. The Au nanocages can be easily synthesized from Ag nanocubes through a galvanic replacement reaction on a sub-gram scale. Simple chemistry allows us to engineer their surface properties through gold-thiolate bonds, followed by conjugation of tumor targeting moieties to the surface. To warrant translation from laboratory research to clinical trials in the future, it is important to demonstrate the capability to produce Au nanocages and their derivatives at low cost, with high reproducibility, and under the good manufacture practice (GMP) guidelines.^[46]

The cellular uptake of Au nanocages largely depends on their size and surface properties. An important future study would also address the interaction at the interface of conjugated nanocages with their receptors, as this may affect cell signaling pathways. For example, nanoparticles functionalized with biomolecules (e.g., antibodies or peptides) cannot only play a role in cellular or organelle targeting, but may also activate cellular signaling pathways that alter protein expressions and the fate of the cell.^[47] For favorable in vivo biodistribution, passive targeting relies on the leaky vasculature of tumors. Some tumors might not be accessible by this targeting mechanism, or greater targeting may be required. In such cases, active targeting with specific recognized ligands may improve the uptake efficiency of the target. It is thus of particular interest to identify cancer-specific biomarkers, as well as understand the interfacial barriers to nanoparticle delivery to the target.

Due to their large absorption cross sections, Au nanocages are ideal candidates as contrast agents for photoacoustic imaging. The detectable depth of PA signals can reach 33 mm, which is adequate for clinical applications. The photothermal effect of Au nanocages can also effectively treat tumors locally. By covering Au nanocages with a smart polymer, the encapsulated drugs or other molecular species can be released remotely with a NIR light trigger. Gold-based nanoparticles are bio-inert and have been under clinical investigation in human studies for drug delivery and laser therapy.^[48] By combining these features together, Au nanocages are expected to become a new platform for cancer diagnosis and treatment.

Acknowledgements

This work was supported in part by a Director's Pioneer Award from the NIH (DP1 OD000798), a research grant (1R01 CA138527) from the NIH, and startup funds from Washington University in St. Louis (to Y.X.), as well as a Research Development Award from the Alvin J. Siteman Cancer Center at Barnes-Jewish Hospital and Washington University School of Medicine (to J.C.). The Siteman Cancer Center is supported by a Grant (P30 CA91842) from the NIH. This article is part of a Special Issue on Nanomaterials Research by Chinese Scientists.

Received: July 1, 2010
Published online: October 4, 2010

- [1] See for example, a) R. A. Sperling, P. R. Gil, F. Zhang, M. Zanella, W. J. Parak, *Chem. Soc. Rev.* **2008**, *37*, 1896; b) P. Ghosh, G. Han, M. De, C. K. Kim, V. M. Rotello, *Adv. Drug Del. Rev.* **2008**, *60*, 1307; c) Robert Wilson, *Chem. Soc. Rev.* **2008**, *37*, 2028; d) E. Boisselier, D. Astruc, *Chem. Soc. Rev.* **2009**, *38*, 1759.
[2] G. J. Higby, *Gold Bull.* **1982**, *15*, 130.

- [3] Research Subcommittee of the Empire Rheumatism Council, *Ann. Rheum. Dis.* **1960**, *19*, 95.
- [4] P. F. Hahn, J. P. B. Goodell, C. W. Sheppard, R. O. Cannon, H. C. Francis, *J. Lab. Clin. Med.* **1947**, *32*, 1442.
- [5] U. Kreibitz, M. Vollmer, *Optical Properties of Metal Clusters*, Vol. 25, Springer, Berlin **1995**.
- [6] See for example, a) P. K. Jain, X. Huang, I. H. El-Sayed, M. A. El-Sayed, *Acc. Chem. Res.* **2008**, *41*, 1578; b) S. E. Skrabalak, J. Chen, Y. Sun, X. Lu, L. Au, C. M. Cobley, Y. Xia, *Acc. Chem. Res.* **2008**, *41*, 1587; c) C. J. Murphy, A. M. Gole, J. W. Stone, P. N. Sisco, A. M. Alkilany, E. C. Goldsmith, S. C. Baxter, *Acc. Chem. Res.* **2008**, *41*, 1721; d) S. Lal, S. E. Clare, N. J. Halas, *Acc. Chem. Res.* **2008**, *41*, 1842.
- [7] R. Weissleder, *Nat. Biotech.* **2001**, *19*, 316.
- [8] M. Hu, J. Y. Chen, Z. Y. Li, L. Au, G. V. Hartland, X. D. Li, M. Marquez, Y. Xia, *Chem. Soc. Rev.* **2006**, *35*, 1084.
- [9] a) Y. Sun, Y. Xia, *J. Am. Chem. Soc.* **2004**, *126*, 3892; b) J. Chen, J. M. McLellan, A. Siekkinen, Y. Xiong, Z. Y. Li, Y. Xia, *J. Am. Chem. Soc.* **2006**, *128*, 14776; c) X. Lu, H.-Y. Tuan, J. Chen, Z.-Y. Li, B. A. Korgel, Y. Xia, *J. Am. Chem. Soc.* **2007**, *129*, 1733; d) M. H. Kim, X. Lu, B. Wiley, E. P. Lee, Y. Xia, *J. Phys. Chem. C* **2008**, *112*, 7872.
- [10] a) B. Wiley, Y. Sun, B. Mayers, Y. Xia, *Chem. Euro. J.* **2005**, *11*, 454; b) Y. Sun, B. Mayers, T. Herricks, Y. Xia, *Nano Lett.* **2003**, *3*, 955.
- [11] a) Y. Sun, Y. Xia, *Science* **2002**, *298*, 2176; b) D. Yu, V. W. Yam, *J. Am. Chem. Soc.* **2004**, *126*, 13200; c) A. Tao, P. Sinsermsuksakul, P. Yang, *Angew. Chem. Int. Ed.* **2006**, *45*, 4597; d) H. Chen, Y. Wang, S. Dong, *norg. Chem.* **2007**, *46*, 10587; e) F. Fan, D. Liu, Y. Wu, S. Duan, Z. Xie, Z. Jiang, Z. Tian, *J. Am. Chem. Soc.* **2008**, *130*, 6949; f) Q. Zhang, C. Z. Huang, J. Ling, Y. F. Li, *J. Phys. Chem. B* **2008**, *112*, 16990.
- [12] a) F. Fievet, J. P. Lagier, M. Figlarz, *MRS Bull.* **1989**, *14*, 29; b) S. E. Skrabalak, B. J. Wiley, M. H. Kim, E. Formo, Y. Xia, *Nano Lett.* **2008**, *8*, 2077.
- [13] B. Wiley, Y. Sun, Y. Xia, *Acc. Chem. Res.* **2007**, *40*, 1067.
- [14] a) B. Wiley, T. Herricks, Y. Sun, Y. Xia, *Nano Lett.* **2004**, *4*, 1733; b) S. H. Im, Y. T. Lee, B. Wiley, Y. Xia, *Angew. Chem. Int. Ed.* **2005**, *117*, 2192.
- [15] a) A. R. Siekkinen, J. M. McLellan, J. Chen, Y. Xia, *Chem. Phys. Lett.* **2006**, *432*, 491; b) Q. Zhang, C. Cobley, L. Au, M. McKiernan, A. Schwartz, L.-P. Wen, J. Chen, Y. Xia, *ACS Appl. Mater. Interfaces* **2009**, *1*, 2044.
- [16] Q. Zhang, W. Li, L.-P. Wen, J. Chen, Y. Xia, *Chem. Euro. J.* **2010**, in press.
- [17] a) X. Lu, J. Chen, S. E. Skrabalak, Y. Xia, *Proc. IMechE Part N: J. Nanoeng. Nanosys.* **2008**, *221*, 1; b) S. E. Skrabalak, L. Au, X. Li, Y. Xia, *Nat. Protoc.* **2007**, *2*, 2182.
- [18] I. Lampre, P. Pernot, M. Mostafavi, *J. Phys. Chem. B* **2000**, *104*, 6233.
- [19] J. C. Love, L. A. Estroff, J. K. Kriebel, R. G. Nuzzo, G. M. Whitesides, *Chem. Rev.* **2005**, *105*, 1103.
- [20] Y. Borodko, S. E. Habas, M. Koebel, P. Yang, H. Frei, G. A. Somorjai, *J. Phys. Chem. B* **2006**, *110*, 23052.
- [21] G. M. Whitesides, P. E. Laibinis, *Langmuir* **1990**, *6*, 87.
- [22] E. C. Cho, L. Au, Q. Zhang, Y. Xia, *Small* **2009**, *6*, 517.
- [23] a) B. Larsen, *Mol. Cell. Biochem.* **1977**, *15*, 117; b) E. Skutelsky, D. Danon, *J. Cell Biol.* **1976**, *71*, 232; c) S. E. Mutsaers, J. M. Papadimitriou, *J. Luek. Biol.* **1988**, *44*, 17; d) M. G. Farquhar, *J. Cell Biol.* **1978**, *78*, R35; e) M. W. Seiler, M. A. Venkatachalam, R. S. Cotran, *Science* **1975**, *189*, 390; f) P. M. Quinton, C. W. Philpott, *J. Cell Biol.* **1973**, *56*, 787.
- [24] a) P. R. Leroueil, S. Hong, A. Mecke, J. R. Baker, Jr, B. G. Orr, M. M. B. Holl, *Acc. Chem. Res.* **2007**, *40*, 335; b) A. Verma, O. Uzun, Y. Hu, Y. Hu, H.-S. Han, N. Watson, S. Chen, D. J. Irvine, F. Stellacci, *Nat. Mater.* **2008**, *7*, 588; c) J. Chen, J. A. Hessler, K. Putchakayala, B. K. Panama, D. P. Khan, S. Hong, D. G. Mullen, S. C. DiMaggio, A. Som, G. N. Tew, A. N. Lopatin, J. R. Baker, Jr, M. M. B. Holl, B. G. Orr, *J. Phys. Chem. B* **2009**, *113*, 11179.
- [25] E. C. Cho, J. Xie, P. A. Wurm, Y. Xia, *Nano Lett.* **2009**, *9*, 1080.
- [26] D. Peer, J. M. Karp, S. Hong, O. C. Farokhzad, R. Margalit, R. Langer, *Nat. Nanotechnol.* **2007**, *2*, 751.
- [27] a) S. M. Moghimi, A. C. Hunter, J. C. Murray, *Pharmacol. Rev.* **2001**, *53*, 283; b) X. Qian, X.-H. Peng, D. O. Ansari, Q. Yin-Goen, G. Z. Chen, D. M. Shin, L. Yang, A. N. Young, M. D. Wang, S. Nie, *Nat. Biotechnol.* **2008**, *26*, 83.
- [28] R. E. Mebius, G. Kraal, *Nat. Rev. Immunology* **2005**, *5*, 606.
- [29] R. K. Jain, *Ann. Rev. Bio. Engineer.* **1999**, *1*, 241.
- [30] C. H. Kim, E. C. Cho, J. Chen, K. H. Song, L. Au, C. Favazza, Q. Zhang, C. M. Cobley, F. Gao, Y. Xia, L. V. Wang, *ACS Nano* **2010**, *4*, 4559.
- [31] L. V. Wang, *Nat. Photonics* **2009**, *3*, 503.
- [32] X. Yang, E. W. Stein, S. Ashkenazi, L. V. Wang, *Wiley Interdiscip. Rev.: Nanomed. Nanobiotechnol.* **2009**, *1*, 360.
- [33] L. V. Wang, H. Wu, *Biomedical Optics: Principles and Imaging*, Wiley, New Jersey **2007**.
- [34] E. C. Cho, C. Kim, F. Zhou, C. M. Cobley, K. H. Song, J. Chen, Z.-Y. Li, L. V. Wang, Y. Xia, *J. Phys. Chem. C* **2009**, *113*, 9023.
- [35] K. H. Song, C. Kim, C. M. Cobley, Y. Xia, L. V. Wang, *Nano Lett.* **2009**, *9*, 183.
- [36] G. Ravizzini, B. Turkbey, T. Barrett, H. Kobayashi, P. L. Choyke, *Wiley Interdiscip. Rev.: Nanomed. Nanobiotechnol.* **2009**, *1*, 610.
- [37] a) M. G. Torchia, R. Nason, R. Danzinger, J. M. Lewis, J. A. Thliveris, *J. Surg. Oncology* **2001**, *78*, 151; b) S. Sohrabnezhad, A. Pourahmad, M. A. Sadjadi, *Mater. Lett.* **2007**, *61*, 2311.
- [38] M. Hu, H. Petrova, J. Chen, J. M. McLellan, A. R. Siekkinen, M. Marquez, X. Li, Y. Xia, G. V. Hartland, *J. Phys. Chem. B* **2006**, *110*, 1520.
- [39] J. L. Roti Roti, *Int. J. Hyperthermia* **2008**, *24*, 3.
- [40] A. Vogel, V. Venugopalan, *Chem. Rev.* **2003**, *103*, 577.
- [41] J. Chen, C. Glaus, R. Laforest, Q. Zhang, M. Yang, M. Gidding, M. J. Welch, Y. Xia, *Small* **2010**, *6*, 811.
- [42] a) C. Pottgen, S. Levegrun, D. Theegarten, S. Marnitz, S. Grehl, R. Pink, W. Eberhardt, G. Stamatis, T. Gauler, G. Antoch, A. Bockisch, M. Stuschke, *Clin. Cancer Res.* **2006**, *12*, 97; b) S. M. Schuetze, J. F. Eary, K. A. Griffith, B. P. Rubin, D. S. Hawkins, C. B. Vernon, G. N. Mann, E. U. Conrad, *J. Clin. Oncology* **2005**, *23* (Suppl.), 9005; c) D. Hellwig, T. P. Graeter, D. Ukena, T. Georg, C.-M. Kirsch, D.-I. H.-J. Schäfers, *J. Thoracic Cardiovascular Surgery* **2004**, *128*, 892.
- [43] M. S. Yavuz, Y. Cheng, J. Chen, C. M. Cobley, Q. Zhang, M. Rycenga, J. Xie, C. Kim, K. H. Song, A. G. Schwartz, L. V. Wang, Y. Xia, *Nat. Mater.* **2009**, *8*, 935.
- [44] A. S. Hoffman, *Adv. Drug Del. Rev.* **2002**, *54*, 3.
- [45] A. Jemal, R. Siegel, E. Ward, Y. Hao, J. Xu, M. J. Thun, *CA-Cancer J. Clin.* **2009**, *59*, 225.
- [46] R. Goel, N. Shah, R. Visaria, G. F. Paciotti, J. C. Bischof, *Nanomedicine*, **2009**, *4*, 401.
- [47] a) A. Verma, F. Stellacci, *Small* **2010**, *6*, 12; b) W. Jiang, B. Y. Kim, J. T. Rutka, W. C. W. Chan, *Nat. Nanotech.* **2008**, *3*, 145; c) B. Kang, M. A. Mackey, M. A. El-Sayed, *J. Am. Chem. Soc.* **2010**, *132*, 1517.
- [48] a) <http://www.cytimmune.com/go.cfm?do=Page.View&pid=19>, (accessed: September, **2010**); b) <http://www.nanospectra.com/clinicians/aurolasetherapy.html>, (accessed: September, **2010**).